Artificial Intelligence in Agriculture 5 (2021) 125–132

Contents lists available at ScienceDirect

Artificial Intelligence in Agriculture

journal homepage: http://www.keaipublishing.com/en/journals/artificial-intelligence-in-agriculture/

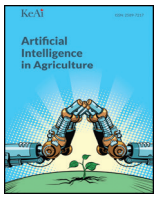

Identification of various food residuals on denim based on hyperspectral imaging system and combination optimal strategy

Yuzhen Chen [a], Ziyi Xu [a,b], Wencheng Tang [c,d], Menghan Hu [a,*], Douning Tang [a,b], Guangtao Zhai [c], Qingli Li [a]

[a] Shanghai Key Laboratory of Multidimensional Information Processing, School of Communication & Electronic Engineering, East China Normal University, Shanghai 200062, China
[b] School of Statistics, East China Normal University, Shanghai 200062, China
[c] Institute of Image Communication and Information Processing, Shanghai Jiao Tong University, Shanghai 200240, China
[d] McCormick School of Engineering, Northwestern University, Evanston, IL, United States

ARTICLE INFO

Article history:
Received 12 May 2021
Received in revised form 20 June 2021
Accepted 20 June 2021
Available online 26 June 2021

Keywords:
Hyperspectral imaging
Food residual on denim
Combination optimal strategy
Variable selection
Forensic application

ABSTRACT

As the science and technology develop, crime methods and scenes have become increasingly complex and diverse. Trace evidence analysis has become a more and more important criminal investigation technology and liquid is the main form of trace evidence. Food can provide not only energy, but clues to solve crimes. In this study, we build a hyperspectral imaging system to detect liquid residue traces, including apple juice, coffee, cola, milk and tea, on denims with light, middle and dark colors. The obtained hyperspectral images are first subjected to spectral calibration and hyperspectral data pretreatment. Subsequently, Partial Least Squares (PLS) is applied to select the informative wavelengths from the preprocessed spectra. For modeling phase, the combination optimal strategy, support vector machine (SVM) combined with random forest (RF), is developed to establish classification models. The experimental results demonstrate that the combination optimal model can achieve TPR, FPR, Precision, Recall, F_1, and AUC of 83.5%, 2.30%, 79.7%, 83.5%, 81.6%, and 94.7% for classifying fabrics contaminated by various food residuals. With respect to the classification of liquid and fabric types, the combination optimal model also yields satisfactory classification performance. In future work, we will expand the types of liquid, and make appropriate adjustment to algorithms for improving the robustness of classification models. This research may play a positive role in the construction of a harmonious society.

1. Introduction

The development of science and technology is a double-edged sword. It does bring security to people's life, on the other hand, it may be also used by criminals, who may go beyond the boundaries of law and morality. Therefore, new technologies should be introduced to the exploration of crime scenes to combat the increasingly complex and volatile crime situation. The analysis of trace material evidence is an important technique in criminal investigation (Sumad-on, 2021). On the one hand, thermal residual is important to analyze the thermal trace information in crime scenes (Ai et al., 2020; Xu et al., 2020; Li et al., 2018), however, the forensic investigator is often asked to find the origin of a certain material, which is found at the crime scene (Klaasse et al., 2021; Palmer, 2016). Liquid is the main form of trace material evidence, including beverages, blood, semen, saliva, urine and sweat. The analysis of trace material evidence presents a major challenge, due to the fact that some liquids left at crime scenes are invisible to the naked eye and the amount is limited or even tiny. Recently, researchers have developed many effective chemical experimental methods for the detection of liquid traces at crime scenes. Tobe et al. introduced that the hexagon OBIT method could be used for DNA analysis and that blood could be detected by spraying luminol on suspicious areas (Tobe and Daeid, 2009). Blum et al. developed stable DNA markers which could reliably identify blood and saliva stains (Blum et al., 2006). Fereja et al. developed a luminol electrochemical luminescent biosensor, which could successfully distinguish blood stains from other stains when embed to a smartphone as the detection device (Fereja et al., 2019). However, chemical testing is inevitably destructive and detrimental to crime scene protection. In addition, most chemical experiments need to be carried out in the laboratory, so the results cannot be directly identified in the criminal scenes, which causes inconvenience to the detection of cases.

As a result, researchers begin to apply non-contact, rapid field measurement methods, such as near infrared spectroscopy (Oravec et al., 2019; Takamura et al., 2018), Raman spectroscopy (Doty and Lednev, 2018a; Rosenblatt et al., 2019) and computer vision, to detect material evidence at crime scenes. For near infrared spectroscopy, Takamura et al. demonstrated a dry urine trace detection method based on Fourier transform attenuated total reflection infrared spectroscopy, which finally indicated the chemical source of gender difference in urine donors (Takamura et al., 2019). Zhao et al. proposed a nondestructive detection

* Corresponding author.
E-mail address: mhhu@ce.ecnu.edu.cn (M. Hu).

https://doi.org/10.1016/j.aiia.2021.06.001

method for identifying blood stains based on near-infrared hyperspectral spectrum and established a blood model with high accuracy (Zhao et al., 2019). In terms of the application of Raman spectroscopy technology, Kyle et al. established a support vector machine discriminant analysis model to correctly predict the age of blood donors with high accuracy (Doty and Lednev, 2018b). Muro et al. developed a non-destructive detection technology using Raman spectroscopy to determine the sex of saliva donors at the scene of a crime with high accuracy (Muro et al., 2016). However, the detection methods mentioned above lack spatial dimension information. Additionally, researchers applied computer vision technology to identify and detect material evidence. Tarawneh proposed a non-contact recognition system to effectively identify low quality fingerprints so the problems were solved that palmprint recognition was difficult in low quality images (Tarawneh et al., 2018). Zhu et al. established a trace detection device based on the principle of reflection transformation imaging, which suggested an important application prospect in criminal investigation (Zhu et al., 2019). Unfortunately, the computer vision technology lacks the information of spectral dimension and the component analysis which are responsive to the spectrum, which is important for crime scene analysis.

Hyperspectral imaging technology is composed of images and spectra. The data acquired by this technology includes three kinds of information viz. space, radiation and spectrum. The technique is widely used in agriculture (Mahesh et al., 2015; Ahmed et al., 2016), medicine (Chiang et al., 2017; Li et al., 2017), remote sensing (Adão et al., 2017; Xue and Baofeng, 2017; Duan et al., 2020), textile (Mirschel et al., 2019; Ryu et al., 2017), environment (Foglini et al., 2019; Olmos et al., 2019), and chemistry (Roberts et al., 2018; Jia-Huan et al., 2018). In the field of medical criminal investigation, Przemys et al. introduced a method for detecting the gunshot residue on the fabric based on hyperspectral technology, which was conducive to collecting evidence at the crime scenes (Głomb et al., 2018). Majda et al. proposed a method to get the age of blood stains by estimating the dry degree of them with the help of hyperspectral imaging technology, which could quickly and effectively distinguish blood stains by time (Majda et al., 2018). Cadd et al. proposed a visible wavelength reflectivity hyperspectral imaging technology, which could clearly identify blood stains on white tiles and even distinguish fingerprints in blood from a variety of other fingerprints in red or brown media (Cadd et al., 2016). Nakamura et al. used hyperspectral technology to measure the fluorescence of potential fingerprints, hence, the visual identification and detection of untreated fingerprints are realized successfully (Nakamura et al., 2015).

It is not reported that hyperspectral imaging technology has been used to detect liquid food residues at crime scenes. Although the suspect cannot be identified directly from the liquid food residue, the uniqueness of the liquid food residue can also provide indirect evidence for the case. By detecting liquid food residues left at the scene, the police can get more details about the case and promote the investigation. Accordingly, this will help to fight against the evil forces, promote the development of intelligent public security system, and create a good public security environment for the construction of a harmonious society.

The objective of this study is to investigate the potential of using hyperspectral reflectance imaging to estimate various food residuals on denims. The main steps are as follows: (1) establish the hyperspectral reflectance imaging to acquire the mean pre-processed spectra of denims contaminated by various food residuals; (2) select the wavelengths particularly related with the food residuals using Partial Least Squares (PLS) algorithm; (3) develop the combination optimal classifiers for classifying and recognizing various food residuals on denims.

2. Materials and methods

2.1. Samples of liquid residuals on denim

To simulate the traces of various liquids that might be left at the crime scenes, a variety of common drinks are selected as the materials for this experiment, including apple juice, Coca-Cola, coffee, oolong tea and milk. Cotton denim fabrics covering light, medium and dark colors are chosen to carry these liquids. To simulate different residual time, we dilute each liquid with different concentrations covering concentrations of 100%, 50%, and 25%. Hence, 15 experimental liquids are obtained viz. apple juice, Coca Cola, coffee, oolong tea and milk with concentration of 100%, 50%, and 25%, respectively. The solutions prepared above are used to contaminate the three colors of fabrics to get 45 experimental groups. Plus 3 groups that are not contaminated, we eventually have 48 experimental groups.

The samples in each of the experimental groups are obtained by soaking the cut fabrics in the prepared solutions. The three colors of cotton denim fabrics are all cut into small squares with the size of 4 cm×4 cm. Five samples are prepared for each material condition mentioned above. After drying, a total of 240 experimental samples including 15 fabrics that are not dyed are obtained. All samples are individually encapsulated in sealed bags with labeled numbers.

2.2. Hyperspectral imaging system

A pushbroom Vis–NIR hyperspectral reflectance imaging system is applied to acquire spectral data of the fabric samples prepared previously. The schematic diagram of imaging system is shown in Fig. 1.

This imaging system is mainly composed of an imaging spectrograph (Imspector V10E, Spectral Imaging Ltd., Finland) attached to a 16-bit charge-coupled detector camera of 1004 (spatial)×1002 (spectral) active pixels (Falcon EM285CL, Raptor Photonics Led., U.K.) and a C-mount lens (Model Xenoplan 1.4/17, Jos. Schneider Optische Werke GmbH, Germany), Osram Tungsten halogen lamp, sample stage, and computer.

The conventional line-scan hyperspectral imaging instruments use the fixed image acquisition module and the moving sample stage for data acquisition. However, in practical scenarios, there may not be a sample stage that can move linearly and reliably. Hence, in our research, the hyperspectral imaging system is specially designed which keeps both the image acquisition module and the sample stage fixed while working. This bistatic hyperspectral imaging architecture is achieved by adding a slit to the lens, and the movement of slit can be controlled by a linear motor (shown in the top right corner of Fig. 1). The hypercube can be collected by controlling the uniform movement of the slit. The maximum distance that the slit can reach is 16 mm.

In the current work, the movement speed of slit is set at 0.8 mm/s. The exposure time and the gain of camera are set to 30 ms and 1, respectively. The illumination intensity of halogen lamp is set at 44 Klux. The hypercube with the spectral range covering 328.81–1113.54 nm with full width at the half maximum of approximately 0.8 nm can be obtained with these imaging parameters.

2.3. Spectral calibration

To reduce the instability of light source in spatial dimension, the obtained hyperspectral reflectance images are required to be subjected to the spectral calibration. The equation below was utilized to correct the raw hyperspectral image:

$$R = \frac{I_r - I_d}{I_w - I_d} \quad (1)$$

where R is the corrected hyperspectral reflectance image, I_r stands for the original hyperspectral reflectance image, I_w represents the reference white image of the square white standard using the corrected exposure time, I_d is the reference dark image obtained using the corrected exposure time.

If the above equation works, the image subtraction operations should be carried out between the images with the same exposure time. Therefore, in Eq. 1, the images in numerator and denominator

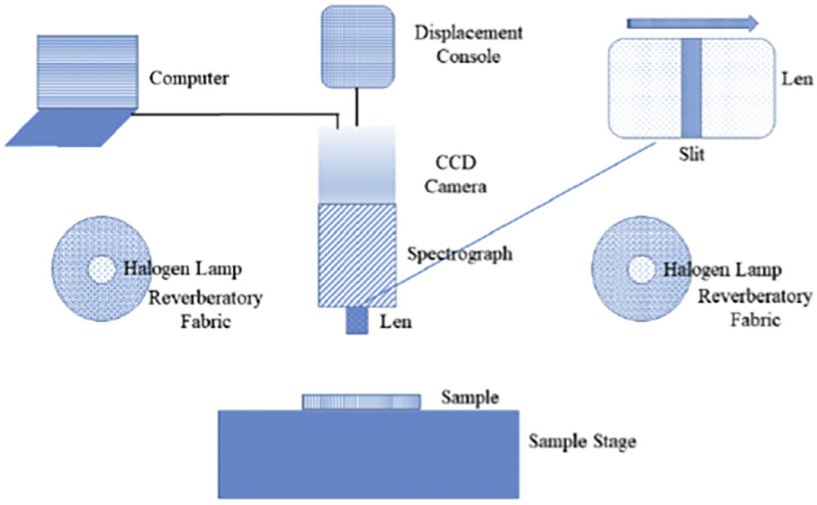

Fig. 1. Schematic diagram of the proposed pushbroom Vis–NIR hyperspectral reflectance imaging system. One of the highlights of this system is that the sample stage keeps still while the slit on the len moves to get the hyperspectral data of sample's different areas.

are respectively captured under working and corrected exposure time. I_d is obtained when the lens cap is closed, and is used primarily to reduce the effects of dark currents in the imaging chip. To guarantee the stability of the calibration process, ten reference white and dark images were acquired each time, and then averaged for correction.

2.4. Hyperspectral data pretreatment

As described above, the distribution of the liquid on the fabric and the composition of the fabric are uniform. Therefore, we ignore the spatial information of the collected hyperspectral data, and only analyze the spectral information. However, the spatial information of hyperspectral image is very useful in practical application scenarios. For example, at an actual crime scene, the location of the liquid residue on the fabric is unknown to us, and we can scan the entire fabric using hyperspectral imaging system to eventually find the exact location of the liquid residue.

For each image, we collected 2000 spectra. Since there were 5 samples for each material condition, a total of 10,000 spectra were ultimately selected for each material condition. For each category, 80% and 20% of spectra were randomly selected as calibration and prediction sets.

To reduce the noise caused by imaging equipment, in this research, the Gauss Low Pass Filter (GLPF) is chosen to convolute the spectral value on the spatial scale, and attenuate the high-frequency components. The GLPF is:

$$H(u,v) = e^{\frac{-D^2(u,v)}{2D_0^2}} \tag{2}$$

$$D(u,v) = \sqrt{(u-u_0)^2 + (v-v_0)^2} \tag{3}$$

where (u,v) is the coordinate of the current pixel. Meantime, $D(u,v)$ is the distance between the current pixel to the center pixel, whose coordinate is (u_0,v_0). D_0 stands for the radius of filter, and it depends on the parameter σ.

To remove the spatial information, we first cropped the hyperspectral image to preserve effectively contaminated areas. A point sampling method commonly used in biological sampling counts called the five-point sampling method was then used to select the valid pixels. The five-point sampling method starts at the center of the image, and then selects the five points that pass through the intersection of the two diagonals at the center and the four corners, together, as representative pixels of the image.

2.5. Characteristic wavelength selection

The extraction of characteristic wavelengths can greatly reduce data redundancy, retain the most representative wavelengths, simplify the model, and speed up model calculation. Partial Least Squares (PLS) removes useless noise and overly tight correlations between data by mapping a high-dimensional original feature vector to a low-dimensional new feature vector. Therefore, PLS is widely used to model linear relationships between samples' attributes and features. Let the output results be $Y_{m\times1}$, and features $X_{m\times p}$. The formulas can be expressed as follows:

$$y = XWc + e = Xb + e \tag{4}$$

where X is the feature matrix; W represents the weight matrix of X; c is the regression coefficient vector and e stands for prediction error. b, which equals $(\mathbf{b_1}, \mathbf{b_2} \ldots \mathbf{b_p})^T$ represents a vector of coefficients in p dimensions.

In matrix b, the absolute value of the ith$(1 \le i \le p)$ element $|b_i|$, indicates how important the ith wavelength is to y. The bigger $|b_i|$ is, the greater its influence on y is. In this research, PLS is employed to extract characteristic wavelengths, and we finally extract 10, 50 and 100 feature wavelengths to model.

2.6. Combination optimal classifier

Support vector machine (SVM) and random forest (RF) algorithms are adopted to construct classification models with training data. Furthermore, we explore the combination of SVM and RF to improve the performance of the ultimate model.

Random forest (Breiman, 2001) is a supervised machine learning algorithm that just emerged in this century. It focuses more on accurately describing the data and classifying them into corresponding categories, as well as summarizing the data. The standard SVM focuses more on binary classification, but it has applied in multi-category classification as well (Belousov et al., 2002). The optimization strategy is shown in Algorithm 1.

Algorithm 1 Procedure of combination strategy

Input: S_{all}: all data set; L_{all}: all labels according to data set;
Output: $(P_{SVM}(best), P_{RF}(best))$: the best parameters of SVM and RF;
Divide S_{all} into S_{train} and S_{test}, and L_{all} into L_{train} and L_{test};
I_i: evaluation indicators of combination strategy; S_{right} and S_{wrong}: the classified right and wrong data; L_{light} and L_{wrong}: the corresponding labels of classified right and wrong data;
for i 1 to max **do**
  $P_{SVM}(i) \leftarrow P_{SVM}(i+1)$;
  Establish $model_{s_i}$ with SVM algorithm based on S_{train}, L_{train}, and $P_{SVM}(i)$;
  for j 1 to max **do**
    $P_{RF}(i) \leftarrow P_{RF}(i+1)$;
    Establish $model_{r_i}$ with RF algorithm using S_{right}, L_{right}, and $P_{RF}(i)$;
    Calculate evaluation indicators I_i using $model_{r_i}$, S_{wrong} and L_{wrong};
Choose the best $(P_{SVM}(best), P_{RF}(best))$ according to all evaluation results I_i;
return $((P_{SVM}(best), P_{RF}(best))$ and $model(best)$

Based on the set proportion, we first divide the all data set S_{all} into training set S_{train}, and test set S_{test}. Then, we train SVM on the S_{train} using the default parameter values of SVM classifier, and test set S_{test} is used to calculate the evaluation indicators to quantize the quality of the model. After training and testing, the classified right samples S_{right} and wrong samples S_{wrong} are respectively assigned with the labels of L_{right} and L_{wrong}. Based on the right samples S_{right} and the obtained SVM classifier, we develop auxiliary classifier RF to get the optimal classification model. It follows the criterion that the evaluation values of classification model can reach the best, which are calculated by classified wrong samples S_{wrong}. More specifically, we assign the parameters generated by randomizer to SVM, and then change the parameters of RF to get the best-performing model. Meanwhile, we record every parameter pair (P_{SVM}, P_{RF}), and eventually we choose the best pair $(P_{SVM}(best), P_{RF}(best))$ to realize optimal model.

2.7. Evaluation indicators

To verify the efficiency of the detection system, evaluation indicators viz. confusion matrix, TPR, FPR, precision, recall, F_1, ROC Curve, AUC are considered.

1) Confusion Matrix: we assume that "Positive" means the positive samples and "Negative" means the negative samples. Meanwhile, "True" represents that the prediction is right while "False" represents that the prediction is wrong. As a result, "TP" and "TN" mean that the positive sample is classified as "Positive" and the negative sample is labeled as "Negative", respectively. "FP" and "FN" represent that the negative sample is labeled as "Positive" and the positive sample is classified as "False". The four indicators make up the confusion matrix.
2) TP Rate (TPR) and FP Rate (FPR): it is a ratio that is used to estimate the classification ability of a model within the range from 0 to 1. They can be calculated by the following equation:

$$TPR = \frac{TP}{TP + FN} \tag{5}$$

$$FPR = \frac{FP}{FP + TN} \tag{6}$$

3) Precision: precision is only used to evaluated the classification ability of the positive samples within the range from 0 to 1. It is obvious that the larger precision is, the more effective the system is. It is computed by:

$$Precision = \frac{TP}{TP + FP} \tag{7}$$

4) Recall: it is a ratio from 0 to 1. Obviously, the more it is close to 1, the better the system is. The calculation equation is:

$$Recall = \frac{TP}{TP + FN} \tag{8}$$

5) F_1: it is a harmonic mean of recall and precision. In this study, we consider the weight of recall and precision the same, which means attaching the weight of 0.5 to either of them. It is calculated by:

$$F_1 = \frac{2 * Precision * Recall}{Precision + Recall} \tag{9}$$

6) ROC Curve and AUC: receiver operating characteristic curve (ROC Curve), is a common indicator to evaluate the advantages and disadvantages of binary classifier. The x-coordinate is FPR, and the y-coordinate is TPR. In general, the closer the ROC curve is to the upper left corner, the better the performance of the classifier is.

Area under curve (AUC) is defined as the area under the ROC Curve. The value of AUC is generally between 0.5 and 1, and the greater the value of AUC is, the better the efficiency of the classifier is.

3. Experimental results and discussion

All work has been finished in Matlab 2014b. With data processed through each step, we analyze the results carefully.

3.1. Results of pretreatment

After pretreatment via Guassian low filtering with different σ, there are different changes in spectral profile. Take the hyperspectral data of pure liquid Coca-Cola as the example, as shown in Fig. 2. It can be seen that there is an increasingly obvious change in the details of the spectrum as σ increases: as σ increases, the details of spectral profiles become less, and the curve becomes smoother viz. many sharp burrs vanish. On the other hand, smoothing also makes the spectrum profile reduces a lot of original features. Therefore, having considered both the processed images and the classification results, the Guassian low pass filter with σ 1 is adopted, which can reach the goal of reducing the burrs and retaining necessary original features.

The Guassian low pass filter with σ 1 is used to process all the simulation materials and the carrier viz. apple juice, Coca-Cola, coffee, oolong tea, milk and light, medium and dark fabrics, which are shown in Fig. 3 and Fig. 4.

Compared with the spectrogram of fabrics, the spectrogram of liquids is much messier. Even after treatment, there is still much burr and sharp bulge, and the curve is more irregular. The spectrogram of coffee, in particular, shares a similar trend with coke, apple juice and tea, perhaps because of their close color similarity.

Among these three kinds of fabrics, it can be seen that there are two peak values in three images. It may be caused by the fact that the

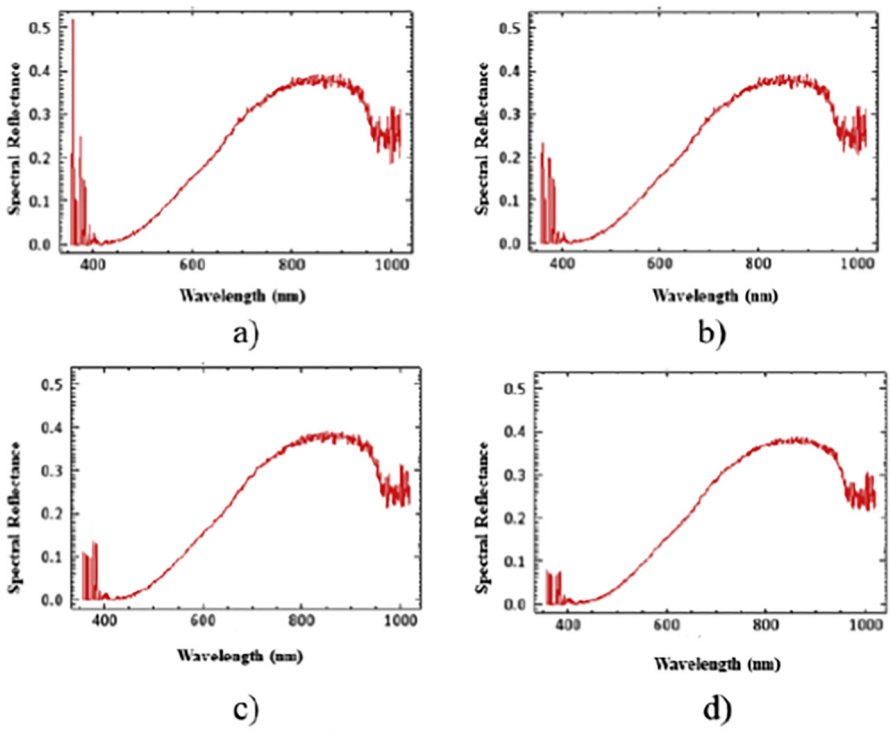

Fig. 2. The spectral profiles of Coca-Cola after pretreatment via Guassian low pass filtering with different σ. Specifically, a) is the original spectral profile while b), c) and d) are the ones that are processed by the Guassian low pass filter with σ 0.5, 1 and 5, respectively.

components of the fabric are more sensitive to the light of two wavebands. With color deepens, the first crest begins to gradually decline, and almost vanishes in terms of dark fabric. Thus, we draw the conclusion that the first wave crest can mainly distinguish the three kinds of fabrics. Meanwhile it may be the characteristic wavelength of these kinds of fabric.

3.2. Analysis of characteristic wavelengths' results

As mentioned above, we use PLS algorithm to extract feature wavelengths after pretreatment. We acquire 10, 50 and 100 characteristic wavelengths and use them respectively to model. The top 100 wavelengths of coffee are elaborated in Fig. 5.

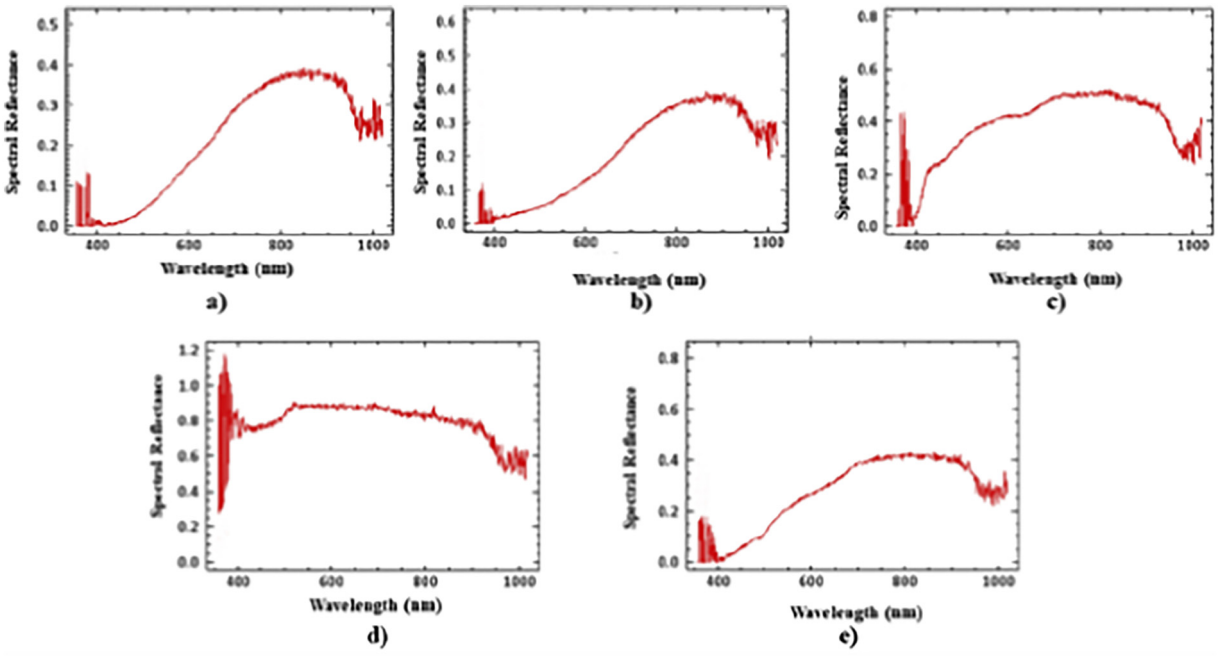

Fig. 3. The spectral profiles of different liquids processed by Guassian low pass filter with σ 1. a), b), c), d) and e) stand for the spectral profiles of Coca-Cola, coffee, apple juice, milk and tea, respectively.

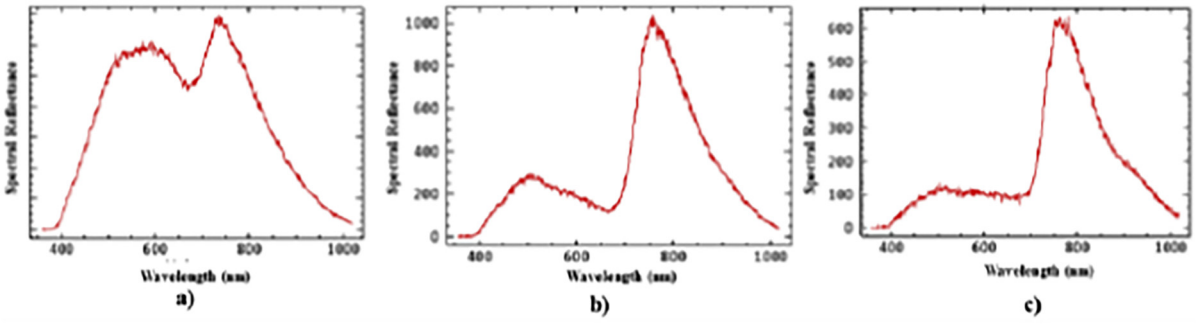

Fig. 4. The spectral profiles of fabrics. a), b) and c) represent the light, medium and dark fabrics, respectively.

As we can see from Fig. 5, the feature wavelengths of top 10 approximately concentrate at 800 nm viz. 1136 cm^{-1}, probably due to the functional group C-Os and C–N 's stretching mode in caffeine, which is the main component in coffee. The feature wavelength of 700 nm viz. 1428 cm^{-1} may come from the functional group C-Hs stretching mode in caffeine and sugar. The other 5 feature wavelengths are probably from other organic matter in coffee. For the top 11 to 50 feature wavelengths, it can be predicted that more characteristics are included. As expected, for the range of 625 nm to 750 nm viz. 1333 cm^{-1} to 1600 cm^{-1}, the wavelengths additionally stand for C=C in stretching mode, while the wavelengths of 780 nm to 830 nm viz.1204 cm^{-1} to 1282 cm^{-1} nm may be attributed to C-Os and C–N 's stretching mode of caffeine. The similar explanation can be applied to the top 51 to 100 feature wavelengths.

The top 10 wavelengths are more reflective of the characteristics of coffee's spectrum; the top 50 can roughly cover the characteristics; and the top 100 can reflect the characteristics more specifically. The characteristic wavelengths of number 10, 50 and 100 are identified by the combination classifier, which are used by random forest and SVM algorithms. When the number of characteristic wavelengths is 50, the classification system performs best. Under the best circumstance, the TP rate is 83.5%, and the FP rate is 2.3% when classifying liquid on denim, which is elaborated in the part 'Performance of Classifiers for Contaminative Denim Classification'.

3.3. Performance of classifiers for liquid category classification

The results of liquid category classification are presented in Table 1. According to Table 1, optimal strategy, as expected, performs better than SVM and RF algorithms. Compared to other indicators, it is easy to observe that the precision of optimal strategy reaches 96.6%, which is the highest and improves most as well. Almost all the evaluation indicators of optimal strategy are promoted except FPR, but it only declines a little. It is very likely that the combination of SVM and RF can obtain a relatively satisfying classification model.

3.4. Performance of classifiers for liquid residue time (concentration) judgment

Table 2 exhibits the classification results of liquid residue time. What stays the same is that the optimal strategy is the one which performs best. It can also be noticed that the performance of all classifiers are

Table 1
Identification Results of Liquid Category by Various Classifiers.

	TPR	FPR	Precision	Recall	F_1	AUC
SVM	85.1%	1.2%	91.0%	85.1%	90.7%	91.4%
RF	84.9%	2.2%	89.5%	84.9%	87.1%	91.2%
Optimal Strategy	86.2%	2.3%	96.6%	86.2%	90.9%	92.2%

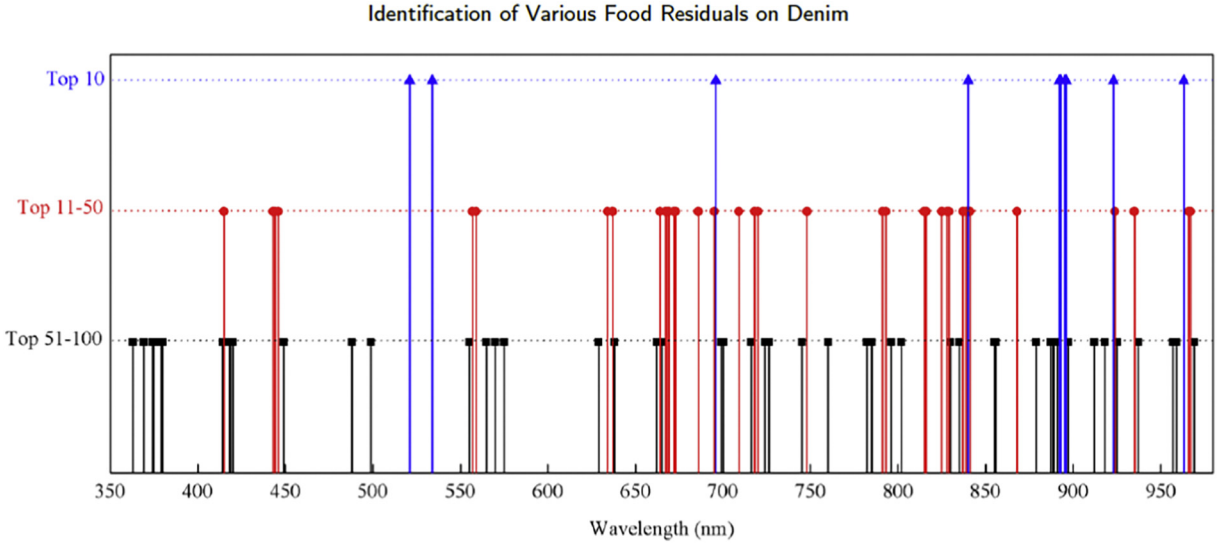

Fig. 5. The top 100 wavelengths of liquid coffee's spectrum. The blue stands for the top 10 wavelengths; the red means top 11 to 51 and the black one represents top 51 to 100.

Table 2
Classification results of liquid residue time (Concentration).

	TPR	FPR	Precision	Recall	F_1	AUC
SVM	72.0%	6.0%	68.9%	72.0%	70.4%	94.3%
RF	73.7%	6.5%	66.4%	73.7%	69.9%	89.4%
Optimal Strategy	76.0%	7.8%	68.5%	76.0%	72.1%	93.5%

Table 3
classification Results of Fabrics with Liquid by Various Classifiers.

	TPR	FPR	Precision	Recall	F_1	AUC
SVM	82.4%	2.7%	78.3%	82.4%	80.3%	93.7%
RF	80.6%	1.8%	82.2%	80.6%	81.4%	91.8%
Optimal Strategy	83.5%	2.3%	79.7%	83.5%	81.6%	94.7%

not as good as the ones classifying the liquid category. It may be caused by the following reasons: 1) excessive classification results in the performance degradation of the classifier; 2) the liquid of the same category but different concentrations consists of essentially the same component, so the hyperspectral difference between the liquids of different concentrations is not enough to distinguish them; 3) the concentration difference is not significant enough, resulting in a relatively small difference after being dried.

In general, the overall performance of the combination method improves the classification system, which shows the feasibility of our classification model.

3.5. Performance of classifiers for contaminative denim classification

Table 3 shows the classification results of fabrics with liquid by various methods. Unsurprisingly, the optimal strategy has the best results on the whole, which proves the combination strategy feasible. It is worth noting that AUC of optimal strategy is approximately close to 95%.

To make it clearer, the specific results of optimal strategy are displayed in Table 4. It can be noted that the system shows a little difference at different categories. TPR of L-Coffee is relatively good, 95.1%, while M-Tea only 70.6%. Fortunately, we can see that the average of all indicators is satisfactory. Positive indicators are all more than 81%, especially AUC is over 91%. The ability of our system to classify multi-category samples is considered to be satisfied.

3.6. Future work in the research

The work can achieve the basic tasks viz. detecting stained cloth with liquid, category of liquid, the kind of cloth, and even the residue time. But owing to the fact that the whole project process is completed in the laboratory, so something that may appear in reality is not considered. So in future work, we should pay more attention to these: 1) the increase in the variety of liquid and cloth will lead to a decrease in the accuracy. In view of the real situation at the crime scene, a high recall rate is required; 2) sample categories need to be expanded. Since the residual liquid on the cloth can be identified only if the liquid is included in the database, it is necessary to add more kinds of liquids; 3) the classification accuracy of different concentrations is relatively low. Since what the hyperspectral reflects is more about the difference between different components, it is necessary to increase the accuracy through appropriate adjustment; 4) we will attempt to use the deep learning to construct classification model; 5) the portability of the system should be taken into consideration. Currently, the system seems a little too large to take into crime scenes. We will try to use multispectral imaging techniques for the construction of relevant models.

Table 4
Classification results of liquid types and contaminated fabric types by optimization strategy.

	TPR	FPR	Precision	Recall	F1	AUC
L-Apple	84.8%	3.9%	81.6%	84.8%	83.1%	93.4%
L-Coffee	95.1%	4.1%	86.5%	95.1%	90.0%	96.0%
L-Cola	78.6%	4.5%	75.9%	78.6%	77.2%	91.9%
L-Milk	78.9%	4.0%	77.7%	78.9%	78.3%	92.1%
L-Tea	72.1%	3.2%	80.0%	72.1%	75.7%	91.4%
M-Apple	72.3%	2.6%	79.7%	76.3%	75.8%	92.7%
M-Coffee	81.5%	3.2%	81.1%	81.5%	81.3%	93.5%
M-Cola	85.2%	2.9%	87.2%	85.2%	86.2%	93.4%
M-Milk	93.0%	0.6%	79.9%	93.0%	85.8%	94.3%
M-Tea	70.6%	3.2%	77.4%	70.6%	73.8%	91.1%
D-Apple	72.8%	5.4%	82.4%	72.8%	77.8%	87.1%
D-Coffee	88.9%	6.8%	85.0%	88.9%	86.9%	91.6%
D-Cola	87.4%	6.9%	87.2%	87.4%	87.3%	89.5%
D-Milk	94.7%	13.6%	81.5%	94.7%	87.4%	92.4%
D-Tea	80.8%	7.60%	78.4%	74.7%	76.5%	87.5%
Average	82.4%	5.2%	81.4%	82.3%	81.5%	91.9%

L, M and D means light, middle and dark fabric.

4. Conclusion

In this work, we develop the hyperspectral imaging system for the detection of liquid residue traces at the crime scene. After gaining hyperspectral images and preprocessing, classifiers viz. SVM and RF, are selected to establish the classification models. Based on these, the optimal combination strategy, SVM combined with RF is chosen to construct model. The system can achieve the tasks of classifying liquid category, liquid concentration, and even different liquid categories on denim. It can be seen from the fact that all positive indicators over 81%, even some over 91% when tackling the most challenging task, detecting different liquid categories on denim. Furthermore, the system performs even better when classifying liquid category and liquid concentration.

Declaration of Competing Interest

The authors declare that there is no conflict of interests regarding the publication of this paper.

Acknowledgements

This work is sponsored by the National Natural Science Foundation of China (No. 61901172, No. 61831015, No. U1908210), the Shanghai Sailing Program (No. 19YF1414100), the “Chenguang Program” supported by Shanghai Education Development Foundation and Shanghai Municipal Education Commission (No. 19CG27), the Science and Technology Commission of Shanghai Municipality (No. 19511120100, No. 18DZ2270700, No. 18DZ2270800), the foundation of Key Laboratory of Artificial Intelligence, Ministry of Education (No. AI2019002), and the Fundamental Research Funds for the Central Universities.

References

Adão, Telmo, Hruška, Jonáš, Pádua, Luís, Bessa, José, Peres, Emanuel, Morais, Raul, Sousa, Joaquim João, 2017. Hyperspectral imaging: a review on uav-based sensors, data processing and applications for agriculture and forestry. Remote Sens. 9 (11), 1110.

Ahmed, Mohammad Raju, Yasmin, Jannat, Mo, Changyeun, Lee, Hoonsoo, Kim, Moon S., Hong, Soon-Jung, Cho, Byoung-Kwan, et al., 2016. Outdoor applications of hyperspectral imaging technology for monitoring agricultural crops: A review. J. Biosyst. Eng. 41 (4), 396–407.

Ai, Jin, Hu, Menghan, Zhai, Guangtao, Zhang, Xiao-Ping, Wang, Yunlu, Cai, Liming, Li, Qingli, Sun, Wendell Q., 2020. Rapidly developing human heat residue model under various conditions based on fluent and thermal video. Infrared Phys. Technol. 110, 103468.

Belousov, A.I., Verzakov, S.A., Von Frese, J., 2002. Applicational aspects of support vector machines. J. Chemometrics: J. Chemometrics Soc. 16 (8–10), 482–489.

Blum, L.J., EsperanÇA, Philippe, Rocquefelte, Stephanie, 2006. A new high-performance reagent and procedure for latent bloodstain detection based on luminol chemiluminescence. J. Can. Soc. Forensic Sci. 39 (3), 81–99.

Breiman, Leo, 2001. Random forests. Mach. Learn. 45 (1), 5–32.

Cadd, Samuel, Li, Bo, Beveridge, Peter, O'Hare, William T., Campbell, Andrew, Islam, Meez, 2016. The non-contact detection and identification of blood stained fingerprints

using visible wavelength reflectance hyperspectral imaging: Part 1. Sci. Justice 56 (3), 181–190.
Chiang, Nathaniel, Jain, Jitendra K., Sleigh, Jamie, Vasudevan, Thodur, 2017. Evaluation of hyperspectral imaging technology in patients with peripheral vascular disease. J. Vasc. Surg. 66 (4), 1192–1201.
Doty, Kyle C., Lednev, Igor K., 2018a. Raman spectroscopy for forensic purposes: recent applications for serology and gunshot residue analysis. TrAC Trends Anal. Chem. 103, 215–222.
Doty, Kyle C., Lednev, Igor K., 2018b. Differentiating donor age groups based on raman spectroscopy of bloodstains for forensic purposes. ACS Central Sci. 4 (7), 862–867.
Duan, Puhong, Lai, Jibao, Kang, Jian, Kang, Xudong, Ghamisi, Pedram, Li, Shutao, 2020. Texture-aware total variation-based removal of sun glint in hyperspectral images. ISPRS J. Photogramm. Remote Sens. 166, 359–372.
Fereja, Tadesse Haile, Kitte, Shimeles Addisu, Gao, Wenyue, Yuan, Fan, Snizhko, Dmytro, Qi, Liming, Nsabimana, Anaclet, Liu, Zhongyuan, Xu, Guobao, 2019. Artesunate-luminol chemiluminescence system for the detection of hemin. Talanta 204, 379–385.
Foglini, Federica, Grande, Valentina, Marchese, Fabio, Bracchi, Valentina A., Prampolini, Mariacristina, Angeletti, Lorenzo, Castellan, Giorgio, Chimienti, Giovanni, Hansen, Ingrid M., Gudmundsen, Magne, et al., 2019. Application of hyperspectral imaging to underwater habitat mapping, southern adriatic sea. Sensors 19 (10), 2261.
Głomb, Przemysław, Romaszewski, Michał, Cholewa, Michał, Domino, Krzysztof, 2018. Application of hyperspectral imaging and machine learning methods for the detection of gunshot residue patterns. Forensic Sci. Int. 290, 227–237.
Jia-Huan, Qu, Wei, Qingyi, Sun, Da-Wen, 2018. Carbon dots: principles and their applications in food quality and safety detection. Crit. Rev. Food Sci. Nutr. 58 (14), 2466–2475.
Klaasse, Jill R., Alewijnse, Linda C., van der Weerd Tracebase, Jaap, 2021. A database structure for forensic trace analysis. Sci. Justice 61 (4), 410–418.
Li, Duo, Zhang, Xiao-Ping, Hu, Menghan, Zhai, Guangtao, Yang, Xiaokang, 2018. Physical password breaking via thermal sequence analysis. IEEE Trans. Inform. Foren. Security 14 (5), 1142–1154.
Li, Xiang, Li, Wei, Xu, Xiaodong, Wei, Hu., 2017. Cell classification using convolutional neural networks in medical hyperspectral imagery. 2017 2nd International Conference on Image, Vision and Computing (ICIVC). IEEE, pp. 501–504.
Mahesh, S., Jayas, D.S., Paliwal, J., White, N.D.G., 2015. Hyperspectral imaging to classify and monitor quality of agricultural materials. J. Stored Prod. Res. 61, 17–26.
Majda, Alicja, Wietecha-Posłuszny, Renata, Mendys, Agata, Wójtowicz, Anna, Łydżba-Kopczyńska, Barbara, 2018. Hyperspectral imaging and multivariate analysis in the dried blood spots investigations. Appl. Phys. A 124 (4), 312.
Mirschel, Gabriele, Daikos, Olesya, Scherzer, Tom, 2019. In-line monitoring of the thickness distribution of adhesive layers in black textile laminates by hyperspectral imaging. Comput. Chem. Eng. 124, 317–325.
Muro, Claire K., de Souza Fernandes, Luciana, Lednev, Igor K., 2016. Sex determination based on raman spectroscopy of saliva traces for forensic purposes. Anal. Chem. 88 (24), 12489–12493.
Nakamura, Atsushi, Okuda, Hidekazu, Nagaoka, Takashi, Akiba, Norimitsu, Kurosawa, Kenji, Kuroki, Kenro, Ichikawa, Fumihiko, Torao, Akira, Sota, Takayuki, 2015. Portable hyperspectral imager with continuous wave green laser for identification and detection of untreated latent fingerprints on walls. Forensic Sci. Int. 254, 100–105.
Olmos, Víctor, Marro, Mónica, Loza-Alvarez, Pablo, Raldúa, Demetrio, Prats, Eva, Piña, Benjamí, Tauler, Romà, De Juan, Anna, 2019. Assessment of tissue-specific multifactor effects in environmental–omics studies of heterogeneous biological samples: combining hyperspectral image information and chemometrics. Talanta 194, 390–398.
Oravec, Michal, Beganović, Anel, Gál, Lukáš, Čeppan, Michal, Huck, Christian W., 2019. Forensic classification of black inkjet prints using fourier transform near-infrared spectroscopy and linear discriminant analysis. Forensic Sci. Int. 299, 128–134.
Palmer, Ray, 2016. The Evaluation of Fibre Evidence in the Investigation of Serious Crime. PhD Thesis. Université de Lausanne, Faculté de Droit, des Sciences Criminelles.
Roberts, Jessica, Power, Aoife, Chapman, James, Chandra, Shaneel, Cozzolino, Daniel, 2018. A short update on the advantages, applications and limitations of hyperspectral and chemical imaging in food authentication. Appl. Sci. 8 (4), 505.
Rosenblatt, Robert, Halámková, Lenka, Doty, Kyle C., de Oliveira Jr., Emanuel A.C., Lednev, Igor K., 2019. Raman spectroscopy for forensic bloodstain identification: method validation vs. environmental interferences. Forensic Chem. 16, 100175.
Ryu, Meguya, Balčytis, Armandas, Wang, Xuewen, Vongsvivut, Jitraporn, Hikima, Yuta, Li, Jingliang, Tobin, Mark J., Juodkazis, Saulius, Morikawa, Junko, 2017. Orientational mapping augmented sub-wavelength hyper-spectral imaging of silk. Sci. Rep. 7 (1), 1–10.
Sumad-on, Donald, 2021. The Methods of Extracting Trace Evidence in Criminal Investigation. Available at SSRN 3832502. .
Takamura, Ayari, Watanabe, Ken, Akutsu, Tomoko, Ozawa, Takeaki, 2018. Soft and robust identification of body fluid using fourier transform infrared spectroscopy and chemometric strategies for forensic analysis. Sci. Rep. 8 (1), 1–10.
Takamura, Ayari, Halamkova, Lenka, Ozawa, Takeaki, Lednev, Igor K., 2019. Phenotype profiling for forensic purposes: determining donor sex based on fourier transform infrared spectroscopy of urine traces. Anal. Chem. 91 (9), 6288–6295.
Tarawneh, Ahmad S., Chetverikov, Dmitry, Hassanat, Ahmad Basheer, 2018. Pilot comparative study of different deep features for palmprint identification in low-quality images. Ninth Hungarian Conference on Computer Graphics and Geometry, Budapest.
Tobe, Shanan S., Daeid, Niamh Nic, 2009. Comparison of presumptive blood test kits including hexagon obti. J. Forensic Sci. 54 (1), 239.
Xu, Ziyi, Wang, Quchao, Li, Duo, Hu, Menghan, Yao, Nan, Zhai, Guangtao, 2020. Estimating departure time using thermal camera and heat traces tracking technique. Sensors 20 (3), 782.
Xue, Jinru, Baofeng, Su., 2017. Significant remote sensing vegetation indices: a review of developments and applications. J. Sens. 2017.
Zhao, Yuefeng, Hu, Nannan, Wang, Yunuan, Liu, Yonglei, Li, Xiaofei, Wang, Jingjing, 2019. The application of near-infrared reflectance hyperspectral imaging for the detection and extraction of bloodstains. Clust. Comput. 22 (4), 8453–8461.
Zhu, Xinran, Huang, Lihua, Wei, Wei, Guo, Kai, Ling, Liqing, Huang, Huijie, 2019. Application of reflection transform imaging in trace detection. 14th National Conference on Laser Technology and Optoelectronics (LTO 2019). vol. 11170. International Society for Optics and Photonics, p. 111702Q.